Article

Bulk and Surface Low Temperature Phase Transitions in the Mg-Alloy EZ33A

Alexander Straumal [1], Ivan Mazilkin [1,2], Kristina Tzoy [1], Boris Straumal [1,2,*], Krzysztof Bryła [3] [iD], Alexander Baranchikov [4] [iD] and Gunther Eggeler [5]

[1] Institute of Solid State Physics RAS, Ak. Ossipyan str. 2, 142432 Chernogolovka, Russia;
a.str@issp.ac.ru (A.S.); mograine@yandex.ru (I.M.); key_tsoy@issp.ac.ru (K.T.)

[2] National University for Science and Technology "MISiS", Leninsky Prospect 4, 119049 Moscow, Russia

[3] Institute of Technology, Pedagogical University of Cracow, Podchorazych str. 2, 30–084 Cracow, Poland;
krzysztof.bryla@up.krakow.pl

[4] Kurnakov Institute of General and Inorganic Chemistry of the Russian Academy of Sciences,
Leninsky Prospect 31, 119991 Moscow, Russia; a.baranchikov@yandex.ru

[5] Ruhr-Universität Bochum, Faculty of Mechanical Engineering, Institute for Materials, Chair for Materials
Science and Engineering, Universitätsstr. 150, D–44780 Bochum, Germany;
gunther.eggeler@ruhr-uni-bochum.de

* Correspondence: straumal@issp.ac.ru; Tel.: +7-916-676-8673

check for updates

Abstract: Low-temperature phase transitions in the EZ33A Mg-cast alloy have been investigated. Based on the structure assessment of the alloy after annealing at 150 °C (1826 h) and at 200 °C (2371 h) a grain boundary wetting transition by a second solid phase was documented. Within a 50 °C temperature range, substantial differences in the α(Mg) grain boundary fraction wetted by the $(Mg,Zn)_{12}RE$ intermetallic were observed. In contrast to what was reported in the literature, two different types of precipitates were found within α(Mg) grains. With increasing annealing temperatures, both types of precipitates dissolved.

Keywords: Mg cast alloy; grain boundaries; precipitation; phase transition; wetting

1. Introduction

In modern materials technology, different Mg-based alloys are used in various applications. This class of materials exhibits low density and good strength. Mg–Zn cast alloys with the addition of different alloying elements represent an important part of this materials class. Quite frequently, in addition to being light weight and strong, these alloys have other beneficial features, like low microporosity and weldability. Unfortunately, they possess low ductility due to brittle intermetallic precipitates which nucleate and grow on grain boundaries (GBs). Many recent investigations [1–3] aim at increasing the ductility of Mg–Zn alloys, by exploring different thermomechanical treatments to reduce cracking.

The scientific objective of the present work is to contribute to these efforts by focusing on the role of wetting surface phase transitions [4]. Special emphasis is placed on the analysis of the solid phase wetting transition and the associated low temperature precipitation processes in the Mg cast alloy EZ33A.

2. Background, Materials and Methods

2.1. Background

The as-cast EZ33A alloy (Figure 1a) has a polycrystalline dendritic structure with a second phase occupying 75% of the GBs and regions in the α(Mg) grain interiors with nanoprecipitates. According to literature, this second phase represents a $(Mg,Zn)_{12}RE$ intermetallic compound [1–3], which has a high hardness and strength. It increases the overall strength of the alloy, especially its creep resistance, by slowing down GB mobility [5,6]. The precipitation in the α(Mg) grain interior results from an increased Zr concentration (saturation) in this region [2,3]. The Zr-saturated areas appear medium-grey in Figure 1a. It is difficult to quantify the chemical composition of the precipitates (highlighted by white arrows with question marks in Figure 1a), as the interaction volume for the energy-dispersive X-ray spectroscopy (EDX) method is larger than the particles. The micrograph in Figure 1b suggests, that 550 °C annealing results in a dissolution of the nanoparticles and a chemical homogenization across the grain [4].
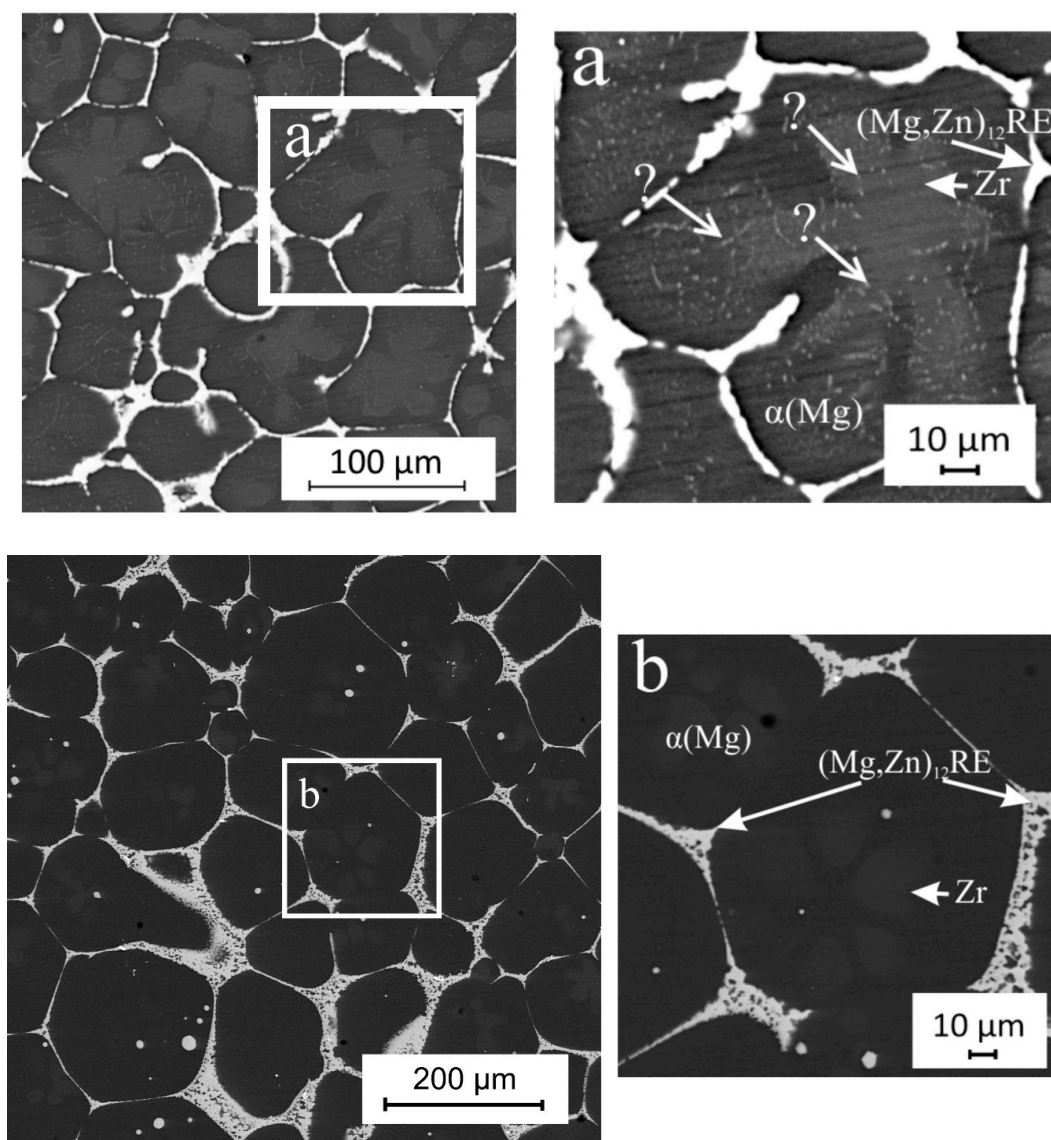

Figure 1. Scanning electron microscope (SEM) micrographs of Mg-cast alloy EZ33A. (**a**) As-cast structure of ingot. White question marks indicate presence of nanoparticles in grain interiors. (**b**) Microstructure after annealing at 550 °C for 2 h [4].

The sample in this figure was annealed at 550 °C for only 2 h, which is a much shorter annealing time than in the experiments of the present work described below. This sample was a part of the previous experimental studies that confirmed the GB wetting phase transition by the second liquid phase in the present alloy in the temperature range from 530 to 590 °C [4]. The short annealing time is explained by the high annealing temperature which results in the partial melting of the structure. The presence of a second liquid phase boosts the diffusion processes significantly and results in shorter transformation times for structure stabilisation. It is clear from Figure 1 that the initial as-cast structure is very similar to the sample structure after a high temperature annealing and subsequent quenching. The similarities of these structures are in detail discussed in [4]. However, the as-cast structure can also be a result of a solid state wetting (spreading) surface phase transition. To examine this possibility long low temperature annealings were performed in this work.

2.2. Material

The investigated EZ33A alloy was provided by the CanMet Materials (Hamilton, ON, Canada). The chemical composition of the material in weight percentage is: 2.5% Zn, 0.4% Zr, 3% rare earth elements (RE), and Mg balance. The RE metals were added to the Mg–Zn–Zr alloy in the form of a 'Mischmetal' addition, consisting mainly of Ce, La, and Nd.

2.3. Methods

Slices that were 2-mm-thick were spark-eroded from the as-cast EZ33A ingot. The ingot and the samples were chemically etched in a 75% HCl + 25% H_2O etching solution. After cutting the samples were encapsulated into evacuated quartz ampoules (residual pressure: 4×10^{-4} Pa) to prevent oxidation. The samples were then subjected to two annealing treatments, 150 °C/1826 h and 200 °C/2371 h. The annealing temperatures and times were chosen specifically to investigate the solid state surface transformations based on the previous experience of the author with such experiments. In both samples, it was expected either to find small numbers of completely wetted grain boundaries to confirm the assumptions or to find a structure similar to the as-cast structure (Figure 1a) which would disprove the existence of the solid state wetting transition. After quenching, the samples were sealed in an electrically conductive resin and mechanically ground and polished.

Polished samples were examined using a LEO 1530 VP scanning electron microscope (SEM) equipped with an Energy-dispersive X-ray (EDX) detector and a backscatter detector (BSD) (LEO Electron Microscopy Inc., Thornwood, NY, USA). The measurements were performed at a working distance of 10 mm and an acceleration voltage of 25 kV. All micrographs of the sample structure were quantified by the Image Expert Pro software (20/20 Software, Inc., Stamford, CT, USA). Values like grain size, number of wetted (covered) by the second phase grain boundaries and surface fractions of the phases were extracted and analyzed. The X-ray diffraction (XRD) method (Siemens D−500 diffractometer, Siemens AG, Munich, Germany) was used to determine the phase composition for all samples.

3. Results and Discussion

XRD patterns demonstrated that all samples contain only two phases, namely the matrix α-(Mg) solid solution phase with a hexagonal crystal structure (P63/mmc) and the second $Mg_{12}RE$ phase with a tetragonal crystal structure (I4/mmm). Figure 2 shows the XRD pattern for the as-cast EZ33A structure. It witnesses the absence of any other phases.

The microstructure after annealing at 150 °C (Figure 3a) reveals significant difference from the initial state. The intermetallic $(Mg,Zn)_{12}RE$ phase has undergone a shape change. Moreover, the volume fraction of the continuous GB second phase layers decreased to only about ~7%. Most of the $(Mg,Zn)_{12}RE$ phase regions, covering 6.2% of the investigated cross section, are situated on GB triple junctions with almost equiaxed and even round particle shapes, and an average particle size of 16 μm.
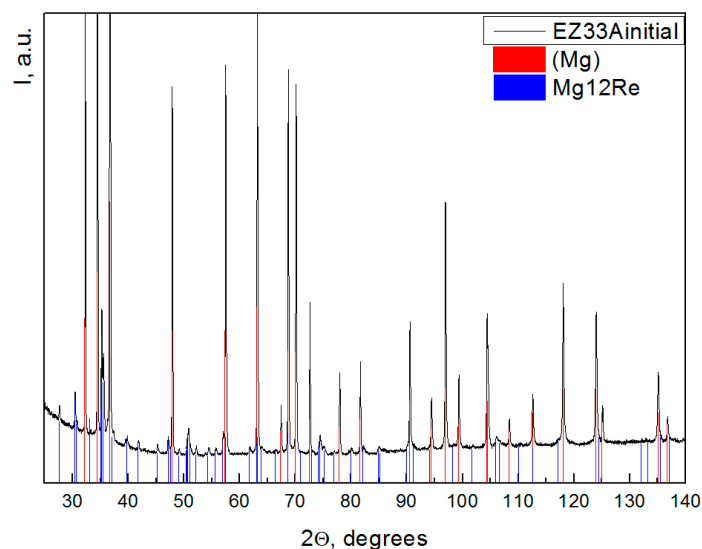
Figure 2. The X-ray diffraction (XRD) pattern for the as-cast EZ33A sample. According to the computer analysis the XRD resolves only two different phases, the matrix α-(Mg) solid solution phase and the second $Mg_{12}RE$ phase.
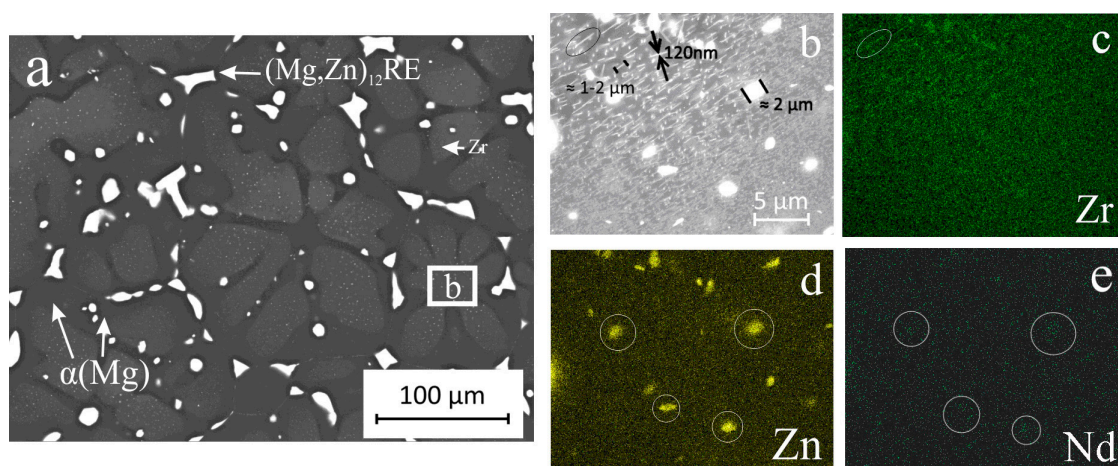

Figure 3. SEM results obtained for Mg-alloy EZ33A after annealing at 150 °C for 1826 h. (**a**) Overall SEM back scatter micrograph. (**b**) SEM back scatter micrograph of the grain interior taken at a higher magnification. Sizes, shapes, and distances between precipitates can be appreciated. Energy-dispersive X-ray spectroscopy (EDX) element distribution maps from microstructural region shown in Figure 3b: (**c**) Zr, (**d**) Zn, and (**e**) Nd.

The precipitates found in the as-cast state have grown in size (Figure 3b). The particle shapes have evolved. One can find lath like, round, and in some cases hexagonal particles of sizes up to 2 μm. These particles do not seem to have a fixed orientation relationship with the matrix. The EDX mappings document a high Zn concentration, moderate concentrations of Zr and Nd and almost no Mg in the $(Mg,Zn)_{12}RE$ particles (Figure 3c–e). Similar precipitates were reported in the literature, after different annealing temperatures and times [5] with higher concentrations of RE [3].

A second type of needle-like precipitates was found in the grain interior (Figure 3b). Unlike the first particle family described so far, these are needle-shaped and do seem to have specific orientations. The size of the needles reached 1–2 μm in length and 120 nm in thickness. The EDX mapping (Figure 3c) allows us to conclude that the small precipitates have a very high Zr concentration. According to the literature these particles might be oriented parallel to the [0001] orientation in the hexagonal Mg lattice. They are the main source of precipitation hardening and creep resistance [7], as the main

dislocation slip systems in hexagonal Mg are microscopic crystallographic slip systems of type {0001} <1,1,−2,0> (basal slip). Some authors suggest [3] that in EZ33A the needle shaped particles represent an intermediate β'_1 phase, which precedes the formation of the lath-shaped β'_2 phase, which was detected in super saturated Mg–Zn and Mg–Zn–RE alloys [8,9]. Based on our EDX mapping results, we suggest that segregation of Zr to the (0001) planes in the α(Mg) hampers the formation of the β'_1 phase in EZ33A and instead promotes the direct formation of the β'_2 lathes.

A new research on the microstructure and mechanical characterization of a ZE41 alloy after equal channel angular pressing (ECAP) deformation, which is an Mg-based alloy very similar to the EZ33A, is reporting a formation of nano-sized $Zr_{22}Zn$ precipitates in the Mg grain interior [10]. The needle-like precipitates could be related to the nano-sized $Zr_{22}Zn$ phase but as the alloys differ in composition, heat treatment and the shape of the particles further certain conclusions can be made only after extensive transmission electron microscopy (TEM) of the EZ33A samples from the present research.

The microstructure after annealing at 200 °C (Figure 4a) shows more similarities to the initial as-cast structure (Figure 1a). The intermetallic $(Mg,Zn)_{12}RE$ phase covers about 81% of the GBs, where it forms continuous layers with a mean thickness of 7 μm. As the microstructure after such long annealing times is close to equilibrium, the difference to the fraction of covered GBs in the first sample confirms the existence of the solid phase GB wetting transition in EZ33A. Similar phenomenon of GBs completely and/or incompletely covered with layers of a second solid phase have been observed also in Al- [11,12], Cu- [13,14], Co- [15], Fe- [16], Zr- [17], and Ti-based alloys [18,19]. Thermodynamically, this phenomenon is very similar to the GB wetting by the melt [20,21].
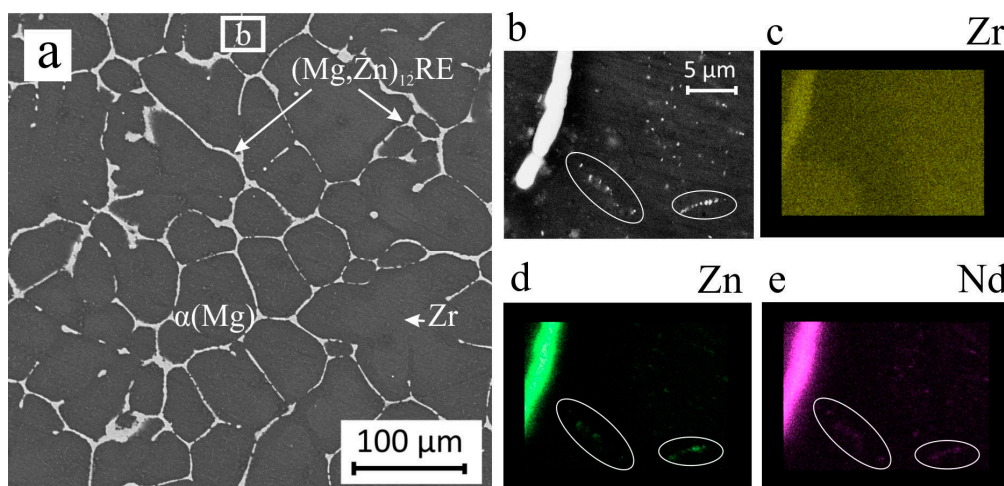

Figure 4. SEM results obtained for Mg-alloy EZ33A after annealing at 200 °C for 2371 h. (**a**) Overall SEM back scatter micrograph. (**b**) SEM back scatter micrograph of the grain interior taken at a higher magnification. Sizes, shapes, and distances between precipitates can be appreciated. EDX element distribution maps from microstructural region shown in Figure 4b: (**c**) Zr, (**d**) Zn, and (**e**) Nd.

It is important to mention that such small temperature interval (50 °C) of the solid phase wetting (spreading) from 7% to 81% of covered GBs in the EZ33A alloy was rather unexpected. In other similar systems the solid state wetting takes place in a much broader temperature range. This can be the result of either a steep surface energy temperature dependence of the solid/solid interface that crosses the different GB energy temperature dependences very fast in the present temperature interval or a very small difference in GB energy of all those GBs that were wetted in the present temperature interval.

Similar to the initial state of the alloy, only the lath-shaped precipitates can be found in the structure (Figure 4b,e). Their size is comparable to the precipitate size in the as-cast state. They are situated in the bright Zr rich area of the α(Mg). Although there appear to be no Zr-precipitates, it is possible that they do not dissolve in α(Mg), but rather are too small to be resolved by a SEM [3].

Previous research results [22] suggest that higher temperatures of the order of 250 °C are required for Zr-precipitates to dissolve and/or significantly shrink.

4. Conclusions

The results obtained in the present work have shown, that grain boundary precipitates redistribution associated with the wetting of GBs occurs in EZ33A. In the 50 °C temperature interval, between 150 °C and 200 °C, the area fraction of wetted GBs rises from 7% to 81%. Two different types of precipitates were found in the grain interior. Needle-shaped Zr-rich particles of 1–2 µm length were all oriented in one direction, presumably [0001]. Lath-shaped hexagonal particles of up to 2 µm diameter were also found, which are enriched in Zn and RE. The existence of the precipitates up to the dissolution at 250 °C provides the high creep resistance.

Conflicts of Interest: The authors declare no conflict of interest.

References

1. Bryła, K.; Morgiel, J.; Faryna, M.; Edalati, K.; Horita, Z. Effect of high-pressure torsion on grain refinement, strength enhancement and uniform ductility of EZ magnesium alloy. *Mater. Lett.* **2018**, *212*, 323–326. [CrossRef]
2. Bryła, K.; Krystian, M.; Horky, J.; Mingler, B.; Mroczka, K.; Kurtyka, P.; Lityńska-Dobrzyńska, L. Improvement of strength and ductility of an EZ magnesium alloy by applying two different ECAP concepts to processable initial states. *Mater. Sci. Eng. A* **2018**, *737*, 318–327. [CrossRef]
3. Rogal, L.; Kania, A.; Berent, K.; Janus, K.; Lityńska-Dobrzyńska, L. Microstructure and mechanical properties of Mg–Zn–RE–Zr alloy after thixoforming. *J. Mater. Res. Technol.* **2019**, *8*, 1121–1131. [CrossRef]
4. Straumal, A.B.; Tsoy, K.V.; Mazilkin, I.A.; Nekrasov, A.N.; Bryła, K. Grain boundary wetting and material performance in an industrial EZ33a Mg cast alloy. *Acta Metall. Mater.* **2019**, *64*, 869–873.
5. Siebert-Timmer, A.; Fletcher, M.; Bichler, L.; Sediako, D. Creep performance of wrought AX30 and EZ33 magnesium alloys. *Can. Met. Quart.* **2013**, *52*, 430–438. [CrossRef]
6. Fletcher, M.; Bichler, L.; Sediako, D.; Klassen, R. Compressive creep behaviour of extruded Mg alloys at 150 °C. In *Magnesium Technology 2011*; Sillekens, W.H., Agnew, S.R., Neelameggham, N.R., Mathaudhu, S.N., Eds.; Springer International Publishing: Cham, Switzerland, 2016; pp. 79–83.
7. Ryspaev, T.; Trojanová, Z.; Padalka, O.; Wesling, V. Microstructure of superplastic QE22 and EZ33 magnesium alloys. *Mater. Lett.* **2008**, *62*, 4041–4043. [CrossRef]
8. Bettles, C.J.; Gibson, M.A. Microstructural design for enhanced elevated temperature properties in sand-castable magnesium alloys. *Adv. Eng. Mater.* **2003**, *5*, 859–865. [CrossRef]
9. Wei, L.Y.; Dunlop, G.L.; Westengen, H. Precipitation hardening of Mg-Zn and Mg-Zn-RE alloys. *MMTA* **1995**, *26*, 1705–1716. [CrossRef]
10. Bryła, K. Microstructure and mechanical characterisation of ECAP-ed ZE41A alloy. *Mater. Sci. Eng. A* **2020**, *772*, 138750. [CrossRef]
11. Straumal, B.B.; Baretzky, B.; Kogtenkova, O.A.; Straumal, A.B.; Sidorenko, A.S. Wetting of grain boundaries in Al by the solid Al_3Mg_2 phase. *J. Mater. Sci.* **2010**, *45*, 2057–2061. [CrossRef]
12. Protasova, S.G.; Kogtenkova, O.A.; Straumal, B.B.; Zięba, P.; Baretzky, B. Inversed solid-phase grain boundary wetting in the Al–Zn system. *J. Mater. Sci.* **2011**, *46*, 4349–4353. [CrossRef]

13. Straumal, B.B.; Kogtenkova, O.A.; Kolesnikova, K.I.; Straumal, A.B.; Bulatov, M.F.; Nekrasov, A.N. Reversible "wetting" of grain boundaries by the second solid phase in the Cu–In system. *Jetp Lett.* **2014**, *100*, 535–539. [CrossRef]

14. Straumal, B.B.; Kogtenkova, O.A.; Straumal, A.B.; Baretzky, B. Grain boundary wetting-related phase transformations in Al and Cu-based alloys. *Lett. Mater.* **2018**, *8*, 364–371. [CrossRef]

15. Straumal, B.B.; Kogtenkova, O.A.; Straumal, A.B.; Kuchyeyev, Y.O.; Baretzky, B. Contact angles by the solid-phase grain boundary wetting in the Co–Cu system. *J. Mater. Sci.* **2010**, *45*, 4271–4275. [CrossRef]

16. Straumal, B.B.; Kucheev, Y.O.; Efron, L.I.; Petelin, A.L.; Dutta Majumdar, J.; Manna, I. Complete and incomplete wetting of ferrite grain boundaries by austenite in the low-alloyed ferritic steel. *J. Mater. Eng. Perform.* **2012**, *21*, 667–670. [CrossRef]

17. Straumal, B.B.; Gornakova, A.S.; Kucheev, Y.O.; Baretzky, B.; Nekrasov, A.N. Grain boundary wetting by a second solid phase in the Zr–Nb alloys. *J. Mater. Eng. Perform.* **2012**, *21*, 721–724. [CrossRef]

18. Gornakova, A.S.; Prokofiev, S.I.; Straumal, B.B.; Kolesnikova, K.I. Growth of (αTi) grain boundary layers in Ti–Co alloys. *Russ. J. Non-Ferr. Met.* **2016**, *57*, 703–709. [CrossRef]

19. Gornakova, A.S.; Straumal, B.B.; Nekrasov, A.N.; Kilmametov, A.; Afonikova, N.S. Grain boundary wetting by a second solid phase in Ti–Fe alloys. *J. Mater. Eng. Perform.* **2018**, *27*, 4989–4992. [CrossRef]

20. Rabkin, E.I.; Shvindlerman, L.S.; Straumal, B.B. Grain boundaries: Phase transitions and critical phenomena. *Int. J. Mod. Phys. B* **1991**, *5*, 2989–3028. [CrossRef]

21. Noskovich, O.I.; Rabkin, E.I.; Semenov, V.N.; Straumal, B.B.; Shvindlerman, L.S. Wetting and premelting phase transitions in 38°[100] tilt grain boundaries in (Fe–12at.%Si) Zn alloy in the vicinity of the A2–B2 bulk ordering in Fe–12at.%Si alloy. *Acta Metall. Mater.* **1991**, *39*, 3091–3098. [CrossRef]

22. Morgan, J.E.; Mordike, B.L. An investigation into creep-resistant, as-cast magnesium alloys containing yttrium, zinc, neodymium and zirconium. *MTA* **1981**, *12*, 1581–1585. [CrossRef]